Research Article Vol. 13, No. 7 / 1 Jul 2023 / Optical Materials Express 2061
Optical Materials EXPRESS

Strain engineering of the electro-optic effect in polycrystalline $BiFeO_3$ films [Invited]

ALFREDO BLÁZQUEZ MARTÍNEZ,[1,2,3] PATRICK GRYSAN,[1] STÉPHANIE GIROD,[1] SEBASTJAN GLINSEK,[1,3] NAVEEN ARUCHAMY,[1,2] PRANAB BISWAS,[2,3] MAEL GUENNOU,[2,3] AND TORSTEN GRANZOW[1,3,*]

[1]*Luxembourg Institute of Science and Technology, Materials Research and Technology Department. 41 rue du Brill, L-4422 Belvaux, Luxembourg*
[2]*Department of Physics and Materials Science, University of Luxembourg. 41 rue du Brill, L-4422 Belvaux, Luxembourg*
[3]*Inter-institutional Research Group Uni.lu–LIST on Ferroic Materials, 41 rue du Brill, L-4422 Belvaux, Luxembourg*
[*]*torsten.granzow@list.lu*

Abstract: Electro-optic thin film materials, which change their refractive index upon the application of an electric field, are crucial for the fabrication of optical modulators in integrated photonic circuits. Therefore, it is key to develop strategies to tune the linear electro-optic effect. Strain engineering has arisen as a powerful tool to optimize the electro-optic coefficients in ferroelectric thin films. In this report, the electro-optical properties of polycrystalline bismuth ferrite ($BiFeO_3$) thin films are studied. The electro-optic coefficients (r_{eff}) of low-cost solution-processed $BiFeO_3$ films under different substrate-induced thermal stress are characterized using a modified Teng-Man technique in transmission geometry. The influence of poling state and substrate stress on the electro-optical properties are discussed. The films show a notable piezo-electro-optic effect: the effective electro-optic coefficient increases both under compressive and tensile in-plane stress, with compressive stress having a much more profound impact. Electro-optic coefficients of 2.2 pm/V are obtained in films under a biaxial compressive stress of 0.54 GPa.

1. Introduction

The control of the propagation of light is a pillar of photonics. With their linear electro-optic (EO) effect, *i.e.*, a linear change of refractive index as a function of an applied electric field, ferroelectric materials are pivotal for this purpose. [1] Progress in the integration of ferroelectric thin film in silicon technology gives a strong incentive to research their EO properties for practical applications. [2,3] Research is concentrated on few promising systems such as barium titanate ($BaTiO_3$, BTO), with high EO coefficients but strong temperature dependence, [4] or (lanthanum-doped) lead zirconate titanate (PZT, PLZT), which is more stable, but subject to environmental legislation restrictions. [1,5] An interesting alternative is bismuth ferrite ($BiFeO_3$, BFO), which is often used in photoferroelectric investigations. [6–10]

Bismuth ferrite is a room temperature multiferroic with ferroelectric and antiferromagnetic ordering. [8,11] In the bulk, it has a Néel temperature T_N around 370 °C [12] and Curie temperature T_C of 810 °C, making it very interesting for high-temperature applications. [8] Indeed, not only its T_C much higher than for BTO or PZT-based compounds, but in addition mode softening is much weaker in general due to the more complex nature of the ferroelectric transition in BFO. [13,14] In addition to the intrinsic linear EO effect, the massive birefringence

#485892 https://doi.org/10.1364/OME.485892
Journal © 2023 Received 17 Jan 2023; revised 24 Mar 2023; accepted 26 Mar 2023; published 23 Jun 2023

Optical Materials EXPRESS

of $BiFeO_3$ of 0.15-0.31, [15,16] allows for refractive index tuning by reorientation of the optical axis through ferroelectric domain switching. The interaction of $BiFeO_3$ with light has been widely studied for photovoltaic (PV) applications due to its low bandgap [17,18] and high remanent polarization. [19,20] The combination of PV and EO properties makes $BiFeO_3$ a potential candidate for photorefractive optics, *i.e.*, changes of refractive index with illumination. So far, PV studies have mostly focused on epitaxial $BiFeO_3$ films; only very recently was the PV behavior of polycrystalline $BiFeO_3$ thin films evidenced to be of bulk photovoltaic (BPV) nature. [6] With respect to the EO properties, values can be found in literature only for epitaxial thin films, reporting effective EO coefficients $\left(r_{\text{eff}} = r_{33} - r_{13}n_{\text{o}}^3/n_{\text{e}}^3\right)$ between 10-15 pm/V. [16,21] There are yet no reports on the EO coefficients of polycrystalline $BiFeO_3$.

Recently, strain engineering has been proposed as a tool to enhance the EO properties. Theoretical studies on the effect of strain on BTO, $SrTiO_3$ and $PbTiO_3$ have shown that the EO properties can be enhanced by the softening of the soft phonon mode through epitaxial strain. [22,23] Kondo et al. reported that the EO coefficient of epitaxial $(Ba_{0.5}Sr_{0.5})TiO_3$ decreases in compressively strained films. [24] However, there is not prediction nor experimental demonstration on the influence of strain on the EO coefficients of $BiFeO_3$ films.

The Teng-Man method is an effective method to determine EO coefficients in reflection geometry. [25] This technique is based on the measurement of the electric-field-induced phase shift between two beam components with mutually perpendicular light polarization. A modification of the Teng-Man set up allows the measurement of EO coefficients in transmission geometry. [16,26] In this geometry, co-planar interdigitated electrodes (IDE) are used to apply uniform in-plane electric fields in absence of a bottom electrode. However, due to the curvature of electric field between the electrodes, special care must be taken in assessing a good balance between the thickness of the material and distance between electrodes in order to probe the whole volume of the material. [27]

In this report, the stress-dependent optical and electro-optical properties of solution-processed polycrystalline $BiFeO_3$ films are studied using the Prism Coupling [28] and the Teng-Man methods. The in-plane stress conditions were varied by choosing substrates with different thermal expansion coefficients, leading to different thermal growth stress. While the zero-field refractive indices of the films vary only minimally with stress, an increase of the effective EO coefficient under both tension and compression is seen. The extrapolated zero-stress value of $r_{\text{eff}} = 1.1$ pm/V increases to 2.2 pm/V under a compressive stress of −0.54 GPa.

2. Thin film growth and optical characterization

Polycrystalline $BiFeO_3$ (BFO) films co-doped with 5 % Mn and 2 % Ti with a thickness of 340 nm were deposited by chemical solution deposition on three different substrates: fused silica, c-cut sapphire (both Siegert Wafer, Germany), and MgO (Biotain Crystal, PR China). The samples based on these substrates will in the following be referred to as BFO/FS, BFO/Sap and BFO/MgO, respectively. The substrates were coated with 23 nm of non-ferroelectric atomic layer deposited HfO_2 films to prevent diffusion during the BFO thin film fabrication. To induce a preferential orientation towards the [100] pseudocubic direction, a seed layer of $PbTiO_3$ was deposited on the substrate prior the deposition of BFO. As shown in [29], the precise doping and a the use of a $PbTiO_3$ seed layer reduce the high-field leakage current of the films, allowing efficient poling. The solutions and the films were prepared according to a standard procedure. [29] The films were crystallized at 600 °C. The in-plane strain of the films is 0.38 % for BFO/FS, 0.10 % for BFO/Sap (tensile) and −0.22 % for BFO/MgO (compressive) as shown in a previous report. [30] Based on a value of 170 GPa for Young's modulus, [31] these strain values correspond to an in-plane tensile stress of (0.93 ± 0.09) GPa for BFO/FS, (0.25 ± 0.03) GPa for BFO/Sap and a compressive stress of (−0.54 ± 0.05) GPa for BFO/MgO.

Optical Materials EXPRESS

The refractive index and thickness of the films was measured using a Metricon model 2010 prism coupler (Metricon, USA). [32–35] Fig. 1(a) shows a schematic of the prism coupling method. A laser beam with wavelength $\lambda = 633$ nm strikes the base of a high refractive index prism (Metricon, Prism 200-P-6-GaP), and is reflected onto a photodetector. The film to be measured is brought into contact with the base of the prism. At certain values of the laser beam's angle of incidence, the photons are guided into optical propagation modes, causing a drop in the intensity of the light striking the photodetector. For a given substrate, the position of the modes only depends on the thickness and the refractive index of the film. The mode equation can be written as: [36]

$$\frac{2\pi}{\lambda} n\cos(\theta)\ T + \Psi_{10} + \Psi_{12} = m\pi\ \ (m = 0,\ 1,\ 2\ldots) \tag{1}$$

where n is the film index, T is the film thickness and Ψ are the Fresnel phase shifts at the BFO/air and BFO/substrate interface. Simultaneous solution of the equation for two modes allows the determination of thickness and refractive index of the film. Figure 1(b) shows the two modes of our BFO thin films on different substrates.

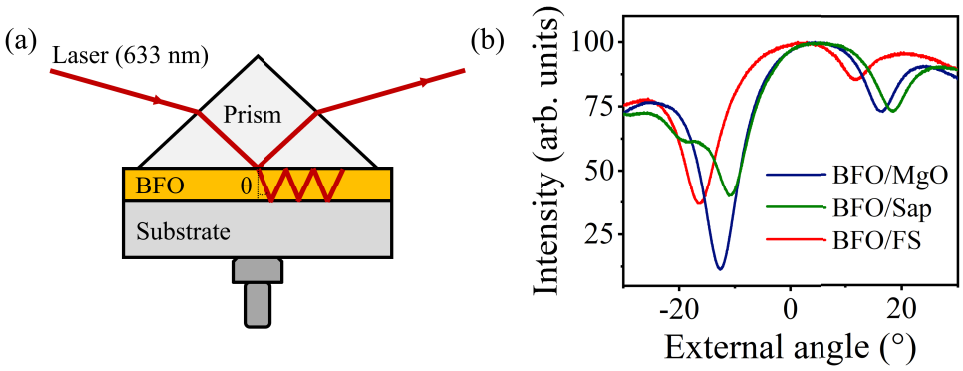

Fig. 1. (a) Sketch of the prism coupling method (b) Intensity vs external angle showing two waveguide modes that allow for the determination of thickness and refractive index of the films

The values for the refractive index and effective average thickness are, respectively, 2.74 ± 0.01 and (339 ± 2) nm in BFO/FS, 2.81 ± 0.01 and (340 ± 2) nm in BFO/Sap and 2.79 ± 0.01 and (342 ± 2) nm in BFO/MgO. The refractive index values are similar to previous reports [16,37] A small change of 2 % in the refractive index is observed under different stress conditions. The films under the lowest stress value shows the largest refractive index. As shown experimentally in [38], the refractive index decreases both with compressive and tensile stress. It is important to note that the refractive index is an average of n_o and n_e, because in a polycrystalline material the optical axes of the individual grains are randomly distributed. In order to discern between n_o and n_e, a preceding poling step must be performed. However, due to the incompatibility of the prism coupling technique with the coplanar electrodes that are needed to pole the film, both of the coefficients cannot be separately measured.

3. Measurements of electro-optic coefficients

To study the EO properties, co-planar IDEs were patterned on top of the BFO films using conventional lift-off photolithography and platinum sputtering. The IDE consist of 50 pairs of fingers with an effective length of 1.5 mm. The width of the fingers is (10 ± 0.5) μm and the space between fingers is (5 ± 0.5) μm. A more detailed description of the device preparation can be found in a previous report. [6] The initial poling procedure consisted of the application

Optical Materials EXPRESS

of a single bipolar triangular field pulse with an amplitude of 1000 kV/cm and a frequency of 1 kHz, while simultaneously recording a ferroelectric $P(E)$ hysteresis loop of polarization as function of electric field. In a second step, additional poling was performed by applying a train of unipolar sinusoidal electric field pulses with an amplitude of either 800 kV/cm or 900 kV/cm and a frequency of 1 kHz during 10 s, for a total of 10,000 poling pulses.

The EO properties were measured using a Teng-Man set up in transmission geometry built in-house, consisting of: a He-Ne laser with a wavelength of 633 nm (Thorlabs, HRS015B), two wire grid polarizers (Thorlabs, WP25M-VIS), a liquid crystal wave retarder (Thorlabs, LCC1423-A) coupled to a liquid crystal controller (Thorlabs, LCC25) and a lock-in amplifier (Zurich Instruments, HF2LI 50 MHz). A schematic of the set-up is shown in Fig. 2.

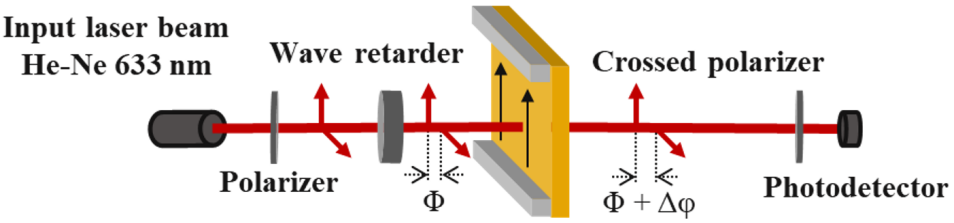

Fig. 2. Schematic of the Teng-Man set-up in transmission geometry

The Teng-Man technique allows for the determination of electro-optic coefficients. [16,25,39] A laser beam with polarization at 45° with respect to the ferroelectric polarization is focused on a sample with interdigitated electrodes. The laser spot size is larger than the distance between two fingers but smaller than the IDE grid (1 mm). The laser is diffracted at the grid, and then, the m = 0 is isolated for the measurement using an iris. The polarized light undergoes a controlled phase shift (Φ) in the wave retarder allowing to shine light with the polarization resulting from a phase shift that ranges from 0 to 2π. The polarized light arrives to the ferroelectric material where an additional phase shift ($\Delta\varphi$) due to the birefringence of the film is produced. The light only goes through the poled region of the film, in which the field is applied in the same direction of the poling. The total phase shift is converted into an intensity modulation using another polarizer aligned at 90° with respect to the first. When an AC signal is applied to the IDE, the phase shift induced by the ferroelectric material changes due to the EO effect. This results in a modulated change of intensity that can be measured using a lock-in amplifier. The mathematical description of the intensity modulation was adapted from [16,40]. The polarization of the light after passing through the crossed polarizers can be written in a Jones formalism as:

$$\mathbf{E}_{\text{out}} = \frac{1}{2}\begin{pmatrix} +1 & -1 \\ -1 & +1 \end{pmatrix}\begin{pmatrix} t_{\parallel} & 0 \\ 0 & t_{\perp} \end{pmatrix}\begin{pmatrix} e^{i\Phi_{\text{LCC}}} & 0 \\ 0 & 1 \end{pmatrix}\begin{pmatrix} 1 \\ 1 \end{pmatrix}\frac{E_0}{2\sqrt{2}} \tag{2}$$

where $t_{\parallel}$ and $t_{\perp}$ are the complex transmission coefficients of the samples for waves with polarization parallel and perpendicular to the direction of the ferroelectric polarization, Φ_{LCC} is the phase shift between $\parallel$ and $\perp$ waves produced by the liquid crystal wave retarder and E_0 is the electric-field amplitude of the incident beam. The voltage generated by the photodiode (V_{PD}) is given by:

$$V_{\text{PD}} = V_0\left[\tau_{\parallel}^2 + \tau_{\perp}^2 - 2\tau_{\parallel}\tau_{\perp}\cos\left(\Phi_{\text{LCC}} + \Phi_{\parallel} - \Phi_{\perp}\right)\right] \tag{3}$$

where $\tau_{\parallel,\perp}$ and $\Phi_{\parallel,\perp}$ are the modulus and argument of the transmission coefficients. Assuming that $\tau_{\parallel,\perp}$ are independent of the applied electric field, when an electric field (E_{elec}) with an amplitude A is applied to the film, the corresponding voltage modulation (V_{LI}) detected by the

Optical Materials EXPRESS

lock-in amplifier is given by:

$$V_{\mathrm{LI}} = A \times \frac{\delta V_{\mathrm{PD}}}{\delta E_{\mathrm{elec}}} \tag{4}$$

$$V_{\mathrm{LI}} = AV_0\left(2\tau_{\parallel}\tau_{\perp}\frac{\delta(\Phi_{\parallel}-\Phi_{\perp})}{\delta E_{\mathrm{elec}}}\sin\left(\Phi_{\mathrm{LCC}}+\Phi_{\parallel}-\Phi_{\perp}\right)\right). \tag{5}$$

The change of phase shift between $\parallel$ and $\perp$ waves when an electric field is applied to the material can be written as:

$$\frac{\delta(\Phi_{\parallel}-\Phi_{\perp})}{\delta E_{\mathrm{elec}}} = \frac{\pi}{\lambda}n_e^3\left(r_{33}-\frac{r_{13}n_0^3}{n_e^3}\right)L_{\mathrm{BFO}} \tag{6}$$

where L_{BFO} is the thickness of the BFO layer affected by the electric field, and n_o and n_e are the ordinary and extraordinary index of BFO, respectively. From Eqs. (3), (5) and (6), the phase change produced by the applied electric field can be expressed as a function of the amplitude of the V_{PD} and V_{LI} curves and r_{eff} can be expressed as:

$$r_{\mathrm{eff}} = r_{33} - r_{13}\frac{n_o^3}{n_e^3} = \frac{\lambda V_{\mathrm{LI}}^0}{\pi n_e^3 L_{\mathrm{BFO}} A V_{\mathrm{PD}}^0} \tag{7}$$

V_{PD} is obtained by measuring the voltage generated by the photodiode without applying an electric field to the sample. The dependence of V_{PD} on the phase shift induced by the liquid crystal wave retarder is measured. The maximum of this V_{PD} curve corresponds to $\Phi + \Delta\varphi = \pi/2$ and the minimum to $\Phi + \Delta\varphi = \pi$. Then, a unipolar sinusoidal AC signal is applied to the interdigitated electrodes, changing the refractive index of BFO, and modifying the change of phase $\Delta\varphi$ that modulates the signal of the photodiode. The change in amplitude and the phase of the signal is recorded by a lock-in technique due to the low signal to noise ratio of the induced change. V_{LI} is recorded as a function of the phase shift induced by the liquid crystal wave retarder.

The theory described above and the possibility to obtain a meaningful electro-optic coefficient in this geometry clearly relies on the assumption that the applied electric field is homogeneous throughout the entire volume of the sample, here the BFO film, which might not be immediately obvious when applying an in-plane field with co-planar IDEs. Figure 3(a) shows the in-plane component of the electric field distribution in the device geometry used in the measurement, numerically simulated by the Finite Element Method with the COMSOL software package, with a voltage of 50 V applied between the IDE fingers. In the current configuration, the electric field in the film is homogeneous between the electrodes. The field also extends a few micrometers into the substrate, but as none of the substrates used had linear EO properties, no contribution will arise from this volume. The penetration of the electric field restricts the measurement configuration to devices where the distance between the electrodes is orders of magnitude larger than the thickness of the material, i.e., thin films. the measurement of bulk materials in this geometry leads to an underestimation of the EO coefficient. To illustrate this limitation, a commercial x-cut $LiNbO_3$ (LNO) single crystal with a thickness of 500 μm and a known effective electro-optic coefficient r_{eff} = 18 pm/V was measured under the same conditions. Co-planar electrodes with a distance of 100 μm were patterned perpendicular to the z axis. A voltage amplitude of 150 V was used in the measurements. The COMSOL simulation of the in-plane electric field distribution inside the crystal is shown in Fig. 3(b). Immediately below the surface, the electric field amplitude is 15 kV/cm as expected. However, the electric field is restricted to the first few micrometers below the surface. The V_{PD} and V_{LI} curves of the $LiNbO_3$ single crystal are shown in Fig. 3(c). Assuming an interaction length of L_{LNO} = 500 μm, *i.e.* the full thickness of the crystal, results in a r_{eff} from the measurement of 0.08 pm/V; the correct value of r_{eff} = 18 pm/V is obtained only for an interaction length of L_{LNO} = 2.2 μm, in agreement with the COMSOL simulation of field

Optical Materials EXPRESS

penetration depth. The use of co-planar structures for the measurement of EO coefficients is therefore restricted to thin films, where the distance between the co-planar electrodes is orders of magnitude larger than the thickness of the film.

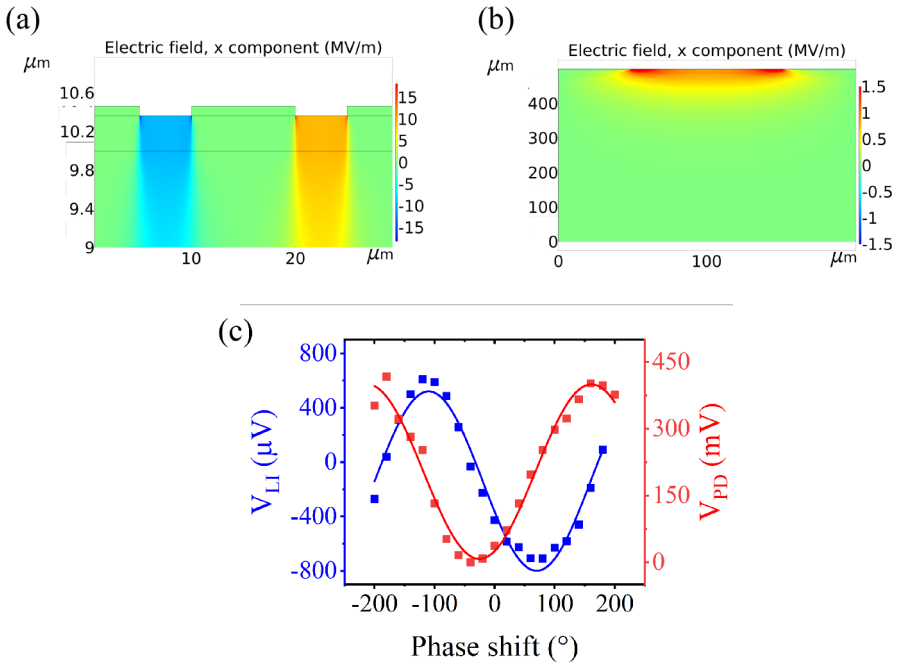

Fig. 3. (a) Modelling of the electric field penetration into a $BiFeO_3$ thin film and (b) into a $LiNbO_3$ single crystal. (c) V_{LI} and V_{PD} curves for a commercial $LiNbO_3$ single crystal with driving field of 15 kV/cm.

An example of the curves from the Teng-Man setup for BFO thin films with an AC electric field of 100 kV/cm can be found in Fig. 4(a). The V_{LI} is smaller than in the $LiNbO_3$ single crystals due to the even shorter path length, which in this case is identical to the film thickness of 340 nm. Figure 4(b) shows the r_{eff} values obtained for BFO films deposited on the three different substrates with different poling treatments. The error bars were calculated by considering the error associated to V_{PD} and V_{LI}, taking into account the stability of the lock-in signal over time and the error in the thickness. Several electrodes were measured obtaining the same values of r_{eff} within the error range. As expected, the unpoled samples do not present a measurable EO coefficient. Before poling, the film is composed of randomly oriented ferroelectric domains, each of which will induce a positive or negative phase shift under an external electric field. The electro-optic response of the macroscopic sample will average out to zero. After poling with a single ferroelectric hysteresis loop with an amplitude of 1000 kV/cm, the domains have a preferred orientation, and their individual electro-optic responses no longer cancel out each other. Values of r_{eff} = 0.3 pm/V are obtained for BFO/Sap, where the lowest level of stress is present. This value increases to r_{eff} = 1.1 pm/V after poling with 10,000 pulses of 800 kV/cm as described above; obviously, the single hysteresis loop is insufficient to achieve poling. When poling with 10,000 pulses of 900 kV/cm, this value increases only slightly to r_{eff} = 1.2 pm/V, indicating that a near-saturation level of poling is reached with this procedure, in agreement with earlier poling studies. [6] The other samples show similar behavior: under higher levels of tensile stress (BFO/FS) the EO coefficient is increased up to 1.4 pm/V after poling at 900 kV/cm. A stronger enhancement of the EO response is observed in the samples under compressive stress

Optical Materials EXPRESS

(BFO/MgO), with values up to 2.2 pm/V. It has to be noted that these values are only about 10 %-15 % of the values reported for single crystals. [16,26] This can be expected due to the polycrystalline nature of the samples: epitaxial thin films typically show better EO properties than polycrystalline ones. [41] The impossibility to achieve full poling of the grains, combined with the lack of in-plane texture that induces a misalignment between the grains, reduce the EO response.

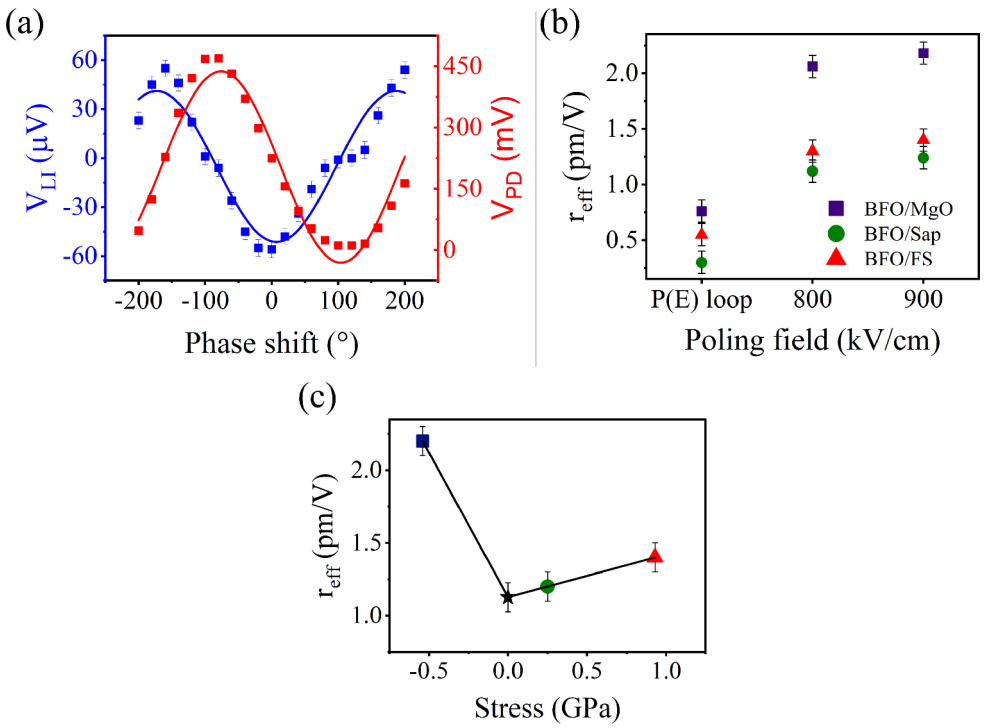

Fig. 4. (a) V_{LI} and V_{PD} curves for BFO/Sap sample poled at 900 kV/cm and a driving field of 100 kV/cm for the measurement of the EO effect. (b) Calculated EO coefficients for BFO films deposited on different substrates with different poling treatment. (c) EO coefficients for BFO after poling at 900 kV/cm. The stress-free EO coefficient is extrapolated from the two samples under tensile stress assuming a linear stress-dependence.

Both compressive and tensile stress increases the EO coefficients in BFO. Assuming that the EO coefficients increase linearly with stress, the zero-stress EO coefficient can be estimated to be 1.1 pm/V. It is understood that a linear extrapolation from two datapoints is only guesswork, but given the relatively low variation of r_{eff} between BFO/Sap with a stress of 0.25 GPa and BFO/FS with a stress of 0.93 GPa, the approach seems reasonable. If this approach is followed, r_{eff} increases with a piezo-EO coefficient of 0.3 $pmV^{-1}GPa^{-1}$ under tensile stress and 2 $pmV^{-1}GPa^{-1}$ under compressive stress.

It seems counterintuitive at first that r_{eff} increases both under tensile and compressive stress. Indeed, for materials like ZnO, an increase of r_{eff} with compression and a decrease with tension was predicted from first-principles calculation. [42] However, this prediction for the uniaxial system ZnO with wurzite structure needs not hold for polyaxial perovskite-structured ferroelectrics. In this case, first-principles studies predict a behavior like the one observed here for $PbTiO_3$ (PTO) [23] and $BaTiO_3$ [22]. Neither of these predictions has so far been experimentally verified. For PTO, the increase under tension is traced to the phonon mode softening at the tetragonal/monoclinic phase transition, while the increase under compression is

Optical Materials EXPRESS

due to electro-mechanical coupling based on the enhanced piezo-response in tetragonal PTO. The stress values observed in the BFO films of the present study are not high enough to induce any phase transition, [43,44], making the mechanism discussed in [23] unlikely. Besides, under different degrees of stress, the poling state of the different films is very similar as shown in [30], in agreement with the expectations for a (001)-oriented rhombohedral perovskite. The most plausible explanation at this point therefore is the enhancement of the EO response due to modifications in the local phonon mode structure that may lead to a mode softening, directly modifying the electro-optic coefficients. [22]

4. Summary and outlook

The EO coefficients (r_{eff}) of solution-processed bismuth ferrite thin films were measured using a custom made Teng-Man set-up in transmission geometry. A strong increase of r_{eff} with stress is observed: with a compressive stress of −0.54 GPa, r_{eff} = 2.2 pm/V were achieved, an increase of about 100 % compared to the extrapolated zero-stress value. The larger piezo-EO coefficient under compressive strain is expected to be even more useful in epitaxially strained $BiFeO_3$ where higher degree of strain can be achieved, e.g., on $DyScO_3$ (−0.8%), $SrTiO_3$ (−1.7%), or $(La_{0.18}Sr_{0.82})(Al_{0.59}Ta_{0.41})O_3$ (−2.4%). [45] Still, solution-processed polycrystalline ferroelectric oxides thin films constitute a low-cost alternative for the development of EO devices.

Besides, the measurements of EO coefficients of the IDE devices together with the BPV effect characterization performed in previous studies [6] allows to assess solution-processed BFO as a candidate for transient photorefractive applications such as reconfigurable waveguides [46,47], i.e. change the refractive index of BFO with above-bandgap illumination. The light-induced change of refractive index can be estimated using the equation given in [47]:

$$\Delta n = -\frac{1}{2} r_{\text{eff}} n^3 E_{ph} \tag{8}$$

The values of Δn can be calculated using the values of photo-induced electric fields (E_{ph}) of 10 kV/cm measured in the films upon illumination of 455 nm with an intensity of 0.48 W/cm^2. [6] At this light intensity, a photoinduced electric field is generated on a short time scale. With an EO coefficient of 2 pm/V, a change of refractive index (Δn) of $2{\cdot}10^{-6}$ can be achieved due to the photo-induced electric field. For comparison, typical values of photoinduced Δn in prototypical $LiNbO_3$ single crystals have a similar order of magnitude of 10^{-5} [48]. Besides, the high dark conductivity of BFO ($\sigma_{\text{Dark}} = 2{\cdot}10^{-7}\ \Omega^{-1}\text{m}^{-1}$) allows the build-up field to decay quickly once the illumination stops, in contrast to what it is observed in $LiNbO_3$. While this would be detrimental for long-time applications like optical data storage, it greatly facilitates short-time applications relying on transient modifications of the refractive index such as optically reconfigurable waveguides. These results highlight the potential of low-cost solution-processed BFO thin films for EO and photorefractive applications.

Funding. Fonds National de la Recherche Luxembourg (PRIDE17/12246511/PACE).

Disclosures. Authors declare that they have no competing interests.

Data Availability. The data that support the findings of this study are available from the corresponding author upon reasonable request.

References

1. K. Uchino, *Ferroelectric Devices, Chapter 8: Electrooptic Devices* (CRC Press, 2009).
2. S. Abel, F. Eltes, and J. E. Ortmann, *et al.*, "Large Pockels effect in micro- and nanostructured barium titanate integrated on silicon," Nat. Mater. **18**(1), 42–47 (2019).
3. F. Eltes, C. Mai, D. Caimi, M. Kroh, Y. Popoff, G. Winzer, D. Petousi, S. Lischke, J. Elliott Ortmann, L. Czornomaz, L. Zimmermann, J. Fompeyrine, and S. Abel, "A $BaTiO_3$-Based Electro-Optic Pockels Modulator Monolithically Integrated on an Advanced Silicon Photonics Platform," J. Lightwave Technol. **37**(5), 1456–1462 (2019).

Optical Materials EXPRESS

4. M. Zgonik, P. Bernasconi, M. Duelli, R. Schlesser, P. Günter, M. H. Garrett, D. Rytz, Y. Zhu, and X. Wu, "Dielectric, elastic, piezoelectric, electro-optic, and elasto-optic tensors of $BaTiO_3$ crystals," Phys. Rev. B **50**(9), 5941–5949 (1994).
5. E.-D. 2002/95/EC, "Restriction of the Use of Certain Hazardous Substances in Electrical and Electronic Equipment (RoHS)," Off. J. Eur. Union **46**, 19–23 (2003).
6. A. Blázquez Martínez, P. Grysan, S. Girod, S. Glinsek, and T. Granzow, "Direct evidence for bulk photovoltaic charge transport in a ferroelectric polycrystalline film," Scr. Mater. **211**, 114498 (2022).
7. H. Matsuo, Y. Noguchi, and M. Miyayama, "Gap-state engineering of visible-light-active ferroelectrics for photovoltaic applications," Nat. Commun. **8**(1), 207 (2017).
8. G. Catalan and J. F. Scott, "Physics and applications of bismuth ferrite," Adv. Mater. **21**(24), 2463–2485 (2009).
9. R. Guo, L. You, Y. Zhou, Z. Shiuh Lim, X. Zou, L. Chen, R. Ramesh, and J. Wang, "Non-volatile memory based on the ferroelectric photovoltaic effect," Nat. Commun. **4**(1), 1990 (2013).
10. A. Bhatnagar, A. Roy Chaudhuri, Y. H. Kim, D. Hesse, and M. Alexe, "Role of domain walls in the abnormal photovoltaic effect in $BiFeO_3$," Nat. Commun. **4**(1), 2835 (2013).
11. R. Ramesh and N. A. Spaldin, "Multiferroics: progress and prospects in thin films, Nat. Mater. **6**, 21–29 (2007).
12. G. S. Kiselev, S. V. Ozerov, and R. P. Zhdanov, "Detection of magnetic order in ferroelectric $BiFeO_3$ by neutron diffraction," Sov. Phys. Dokl. **7**, 742–744 (1963).
13. S. Kamba, D. Nuzhnyy, M. Savinov, J. Šebek, J. Petzelt, J. Prokleška, R. Haumont, and J. Kreisel, "Infrared and terahertz studies of polar phonons and magnetodielectric effect in $BiFeO_3$," Phys. Rev. B **75**(2), 024403 (2007).
14. R. P. S. M. Lobo, R. L. Moreira, D. Lebeugle, and D. Colson, "Infrared phonon dynamics of a multiferroic $BiFeO_3$ single crystal," Phys. Rev. B **76**(17), 172105 (2007).
15. S. Chu, D. Singh, J. Wang, E.-P. Li, and K. Ong, "High optical performance and practicality of active plasmonic devices based on rhombohedral $BiFeO_3$," Laser Photonics Rev. **6**(5), 684–689 (2012).
16. D. Sando, P. Hermet, J. Allibe, J. Bourderionnet, S. Fusil, C. Carrétéro, E. Jacquet, J.-C. Mage, D. Dolfi, A. Barthélémy, P. Ghosez, and M. Bibes, "Linear electro-optic effect in multiferroic $BiFeO_3$ thin films," Phys. Rev. B **89**(19), 195106 (2014).
17. M. C. Weber, M. Guennou, C. Toulouse, M. Cazayous, Y. Gillet, X. Gonze, and J. Kreisel, "Temperature evolution of the band gap in $BiFeO_3$ traced by resonant Raman scattering," Phys. Rev. B **93**(12), 125204 (2016).
18. D. Sando, C. Carrétéro, M. N. Grisolia, A. Barthélémy, V. Nagarajan, and M. Bibes, "Revisiting the Optical Band Gap in Epitaxial $BiFeO_3$ Thin Films," Adv. Opt. Mater. **6**(2), 1700836 (2018).
19. D. Lebeugle, D. Colson, A. Forget, and M. Viret, "Very large spontaneous electric polarization in $BiFeO_3$ single crystals at room temperature and its evolution under cycling fields," Appl. Phys. Lett. **91**(2), 022907 (2007).
20. S.-H. Baek, C. M. Folkman, J.-W. Park, S. Lee, C.-W. Bark, T. Tybell, and C.-B. Eom, "The Nature of Polarization Fatigue in $BiFeO_3$," Adv. Mater. **23**(14), 1621–1625 (2011).
21. M. Zhu, Z. Du, Q. Liu, B. Chen, S. H. Tsang, and E. H. T. Teo, "Ferroelectric $BiFeO_3$ thin-film optical modulators," Appl. Phys. Lett. **108**(23), 233502 (2016).
22. K. D. Fredrickson, V. V. Vogler-Neuling, K. J. Kormondy, D. Caimi, F. Eltes, M. Sousa, J. Fompeyrine, S. Abel, and A. A. Demkov, "Strain enhancement of the electro-optical response in $BaTiO_3$ films integrated on Si(001)," Phys. Rev. B **98**(7), 075136 (2018).
23. C. Paillard, S. Prokhorenko, and L. Bellaiche, "Strain engineering of electro-optic constants in ferroelectric materials," npj Comput. Mater. **5**(1), 6 (2019).
24. S. Kondo, T. Yamada, A. K. Tagantsev, P. Ma, J. Leuthold, P. Martelli, P. Boffi, M. Martinelli, M. Yoshino, and T. Nagasaki, "Large impact of strain on the electro-optic effect in $(Ba,Sr)TiO_3$ thin films: Experiment and theoretical comparison," Appl. Phys. Lett. **115**(9), 092901 (2019).
25. C. C. Teng and H. T. Man, "Simple reflection technique for measuring the electro-optic coefficient of poled polymers," Appl. Phys. Lett. **56**(18), 1734–1736 (1990).
26. M. Zhu, Z. Du, L. Jing, A. I. Yoong Tok, and E. H. Tong Teo, "Optical and electro-optic anisotropy of epitaxial PZT thin films," Appl. Phys. Lett. **107**(3), 031907 (2015).
27. R. Nigon, T. M. Raeder, and P. Muralt, "Characterization methodology for lead zirconate titanate thin films with interdigitated electrode structures," J. Appl. Phys. **121**(20), 204101 (2017).
28. T. W. Hou and C. J. Mogab, "Plasma silicon oxide films on garnet substrates: measurement of their thickness and refractive index by the prism coupling technique," Appl. Opt. **20**(18), 3184 (1981).
29. A. Blázquez Martínez, N. Godard, N. Aruchamy, C. Milesi-Brault, O. Condurache, A. Bencan, S. Glinsek, and T. Granzow, "Solution-processed $BiFeO_3$ thin films with low leakage current," J. Eur. Ceram. Soc. **41**(13), 6449–6455 (2021).
30. A. Blázquez Martínez, P. Grysan, S. Girod, S. Glinsek, and T. Granzow, "Stress-tuning the bulk photovoltaic response in polycrystalline bismuth ferrite films," Appl. Phys. Lett. **122**(15), 152903 (2023).
31. S.-R. Jian, H.-W. Chang, Y.-C. Tseng, P.-H. Chen, and J.-Y. Juang, "Structural and nanomechanical properties of $BiFeO_3$ thin films deposited by radio frequency magnetron sputtering," Nanoscale Res. Lett. **8**(1), 297 (2013).
32. W. H. G. Horsthuis and G. J. M. Krijnen, "Simple measuring method for electro-optic coefficients in poled polymer waveguides," Appl. Phys. Lett. **55**(7), 616–618 (1989).
33. B. A. Smith, S. Herminghaus, and J. D. Swalen, "Electrooptic Coefficients in Electric Field Poled Polymer Waveguides," MRS Proc. **228**, 111 (1991).

Optical Materials EXPRESS

34. A. Boudrioua, E. Dogheche, D. Remiens, and J. C. Loulergue, "Electro-optic characterization of (Pb,La)TiO_3 thin films using prism-coupling technique," J. Appl. Phys. **85**(3), 1780–1783 (1999).
35. B. Chen, P.-R. Hua, S.-Y. Xu, D.-Y. Yu, E. Y.-B. Pun, and D.-L. Zhang, "Mode Indices Measurement of a Special Ti-Diffused $LiNbO_3$ Waveguide Structure: A Strip Waveguide Array Embedded in a Planar Waveguide," IEEE Photonics J. **4**(5), 1553–1559 (2012).
36. P. K. Tien, R. Ulrich, and R. J. Martin, "Modes of propagating light waves in thin deposited semiconductor films," Appl. Phys. Lett. **14**(9), 291–294 (1969).
37. A. Kumar, R. C. Rai, N. J. Podraza, S. Denev, M. Ramirez, Y. H. Chu, L. W. Martin, J. Ihlefeld, T. Heeg, J. Schubert, D. G. Schlom, J. Orenstein, R. Ramesh, R. W. Collins, J. L. Musfeldt, and V. Gopalan, "Linear and nonlinear optical properties of $BiFeO_3$," Appl. Phys. Lett. **92**(12), 121915 (2008).
38. D. Sando, Y. Yang, E. Bousquet, C. Carrétéro, V. Garcia, S. Fusil, D. Dolfi, A. Barthélémy, P. Ghosez, L. Bellaiche, and M. Bibes, "Large elasto-optic effect and reversible electrochromism in multiferroic $BiFeO_3$," Nat. Commun. **7**(1), 10718 (2016).
39. E. Nitiss, A. Bundulis, A. Tokmakov, J. Busenbergs, E. Linina, and M. Rutkis, "Review and comparison of experimental techniques used for determination of thin film electro-optic coefficients," Phys. Status Solidi A **212**(9), 1867–1879 (2015).
40. D. Park, "Characterization of Linear Electro-Optic Effect of Poled Organic Thin Films," Ph.D. thesis (2008).
41. D. Sando, Y. Yang, C. Paillard, B. Dkhil, L. Bellaiche, and V. Nagarajan, "Epitaxial ferroelectric oxide thin films for optical applications," Appl. Phys. Rev. **5**(4), 041108 (2018).
42. C. Li, F. Yang, and W. L. Guo, "Strain-induced modulations of electro-optic and nonlinear optical properties of ZnO: a first-principles study," Appl. Mech. Mater. **29-32**, 1803–1808 (2010).
43. M. Guennou, P. Bouvier, G. S. Chen, B. Dkhil, R. Haumont, G. Garbarino, and J. Kreisel, "Multiple high-pressure phase transitions in $BiFeO_3$," Phys. Rev. B **84**(17), 174107 (2011).
44. D. Sando, A. Barthélémy, and M. Bibes, "$BiFeO_3$ epitaxial thin films and devices: past, present and future," J. Phys.: Condens. Matter **26**(47), 473201 (2014).
45. I. C. Infante, S. Lisenkov, B. Dupé, M. Bibes, S. Fusil, E. Jacquet, G. Geneste, S. Petit, A. Courtial, J. Juraszek, L. Bellaiche, A. Barthélémy, and B. Dkhil, "Bridging Multiferroic Phase Transitions by Epitaxial Strain in $BiFeO_3$," Phys. Rev. Lett. **105**(5), 057601 (2010).
46. P. Dittrich, G. Montemezzani, P. Bernasconi, and P. Günter, "Fast, reconfigurable light-induced waveguides," Opt. Lett. **24**(21), 1508 (1999).
47. F. Juvalta, B. Koziarska-Glinka, M. Jazbinsek, G. Montemezzani, K. Kitamura, and P. Günter, "Deep UV light induced, fast reconfigurable and fixed waveguides in Mg doped $LiTaO_3$," Opt. Express **14**(18), 8278 (2006).
48. Y. Kong, S. Liu, and J. Xu, "Recent advances in the photorefraction of doped lithium niobate crystals," Materials **5**(10), 1954–1971 (2012).